Biophys Rep 2025, 11(5):291–301
https://doi.org/10.52601/bpr.2025.250008 https://cstr.cn/32402.14.bpr.2025.250008
Biophysics Reports
METHOD
Special Topic - CONTROLLED NANOMEDICINE MATERIALS

Construction of genetically encoded biosensors for monitoring cytosolic and mitochondrial H_2O_2 in response to nanozymes in THP-1 cells

Tao Wang[1#], Mengfan Yu[1#], Chenshuo Ren[2,3], Fan Yang[1], Tao Wen[1], Xian-En Zhang[2,4], Haoan Wu[5], Yu Zhang[5], Dianbing Wang[2] ✉, Haiyan Xu[1] ✉

[1] Institute of Basic Medical Sciences, Chinese Academy of Medical Sciences & Peking Union Medical College, Beijing 100005, China
[2] Key Laboratory of Biomacromolecules (CAS), National Laboratory of Biomacromolecules, CAS Center for Excellence in Biomacromolecules, Institute of Biophysics, Chinese Academy of Sciences, Beijing 100101, China
[3] University of Chinese Academy of Science, Beijing 100049, China
[4] Faculty of Synthetic Biology, Shenzhen University of Advanced Technology, Shenzhen 518055, Guangdong, China
[5] State Key Laboratory of Bioelectronics, Jiangsu Key Laboratory for Biomaterials and Devices, School of Biological Science and Medical Engineering & Collaborative Innovation Center of Suzhou Nano Science and Technology, Southeast University, Nanjing 211189, China

Received: 26 January 2025 / Accepted: 28 April 2025

Abstract Intracellular H_2O_2 levels are tightly regulated and can be modulated by various stimuli. A variety of nanozymes have been revealed with the ability to catalyze substrates of oxidoreductases, mostly including peroxidase (POD), superoxide dismutase (SOD) and catalase (CAT), and some of them display multienzyme-like properties, which make them highly attractive for biomedical applications. However, the specific manifestations of nanozyemes within cells remain challenging to predict and detect. In this study, we developed a real-time, dynamic, and highly sensitive live-cell biosensor by expressing HyPer7 probe in the cytosol and mitochondria to monitor the cytosolic and mitochondrial H_2O_2 dynamics in a leukemia cell line THP-1. The successful expression of the probes in the cytosol and mitochondria was confirmed using confocal fluorescence microscopy. When the THP-1 cells were exposed to exogenous H_2O_2, the fluorescence intensity at 525 nm upon excitation with 405 nm lasers (referred to as F405) decreased, while that upon excitation with 488 nm lasers (referred to as F488) increased. Using this biosensor, we examined the dynamics of cytosolic and mitochondrial H_2O_2 in response to Daunorubicin, Fe_3O_4 nanozyme with Polyetherimide (PEI)- or Dextran (Dex)-modification, and Prussian blue nanozyme with different diameters. Results indicated that the particle size of PBNPs and surface modification of Fe_3O_4 play critical roles in their intracellular effects on the aspect of H_2O_2 modulation. The live-cell biosensors thus provide a powerful tool for detecting the variations of cytosolic and mitochondrial H_2O_2 in response to nanozymes, thereby facilitating a better understanding of the biological effects of nanozymes and their potential biomedical applications.

Keywords H_2O_2, Nanozymes, Oxidoreductase, Biosensors

INTRODUCTION

Reactive oxygen species (ROS), which originate from molecular oxygen and are produced through redox

# Tao Wang and Mengfan Yu contributed equally to this work.

✉ Correspondence: wangdb@ibp.ac.cn (D. Wang), xuhy@pumc.edu.cn (H. Xu)

reactions or electronic excitation, have attracted widespread research attention due to their contentious effects (Sies *et al.* 2022). ROS are believed to play a role in oxygen toxicity owing to their heightened chemical reactivity. Moreover, they act as intracellular signaling molecules, taking part in various physiological and pathological processes (D'Autréaux and Toledano 2007; Sies *et al.* 2024). In recent years, it has become evident that using ROS as a blanket term is somewhat imprecise, given that each type of reactive oxygen species possesses distinct properties and functions (Murphy *et al.* 2022; Sies and Jones 2020).

Among the diverse ROS molecules, hydrogen peroxide (H_2O_2) stands out as the primary ROS involved in the redox regulation of biological activities. H_2O_2 serves as a versatile and pleiotropic physiological signaling agent, functioning as a second messenger in biological processes by reversibly oxidizing specific protein thiolates (Sies and Jones 2020). The intracellular concentration of H_2O_2 is maintained in the low nanomolar range (approximately 1–100 nmol/L) and is under tight control (Parvez *et al.* 2018). H_2O_2 is produced from various sources within cells, including specific enzymatic sources such as NADPH oxidases (NOXs) (Bedard and Krause 2007), as well as the mitochondrial electrons transport chains (Murphy 2009), and removed via several intrinsic anti-oxidant small molecules and enzymes, including the thioredoxin system and the glutathione system. Other oxidoreductase can also modulate the intracellular H_2O_2 concentration, including peroxidases (POD), superoxide dismutase (SOD), and catalase (CAT). These properties modulated ROS towards different directions, for example, POD catalyzes the oxidation of substrates in the presence of peroxides (mostly H_2O_2 with a few as organic hydroperoxides) (Jiang *et al.* 2019), therefore consuming hydrogen peroxide to generate other oxides, while SODs disproportionates superoxide radicals into oxygen and H_2O_2 (Jiang *et al.* 2019) to increase the concentration of hydrogen peroxide, and catalase accelerates the dismutation of H_2O_2 into water and oxygen (Jiang *et al.* 2019), therefore scavenging local H_2O_2.

It has been well documented that nanozymes hold the ability to catalyze specific biochemical reactions, showing effects similar to natural enzymes (Ren *et al.* 2022). The most commonly exhibited properties of nanozymes were oxidoreductase-like activity (Jiang *et al.* 2019), including peroxidases (POD), superoxide dismutase (SOD), and catalase (CAT). Many nanozymes, such as metal (Guan *et al.* 2024), metal oxides (Gao *et al.* 2007) and Prussian Blue nanoparticles (Zhang *et al.* 2016), even exhibit multienzyme-like properties in modulating ROS. However, the specific manifestations of nanozymes within cells remain difficult to predict and detect, because different physicochemical properties lead to differences in intracellular distributions and predominant activities. Therefore, it would be beneficial to monitor the dynamics of H_2O_2 of certain organelles for understanding the intracellular activity of nanozymes, especially those that exhibit oxidoreductase-like activities.

Monocytes as part of the innate immune system are one of the first immune cells that are at the sites of infections contributing to pathogen defense with phagocytosis, cytokine and reactive oxygen species (ROS) production. THP-1 monocytes, isolated from the peripheral blood of a boy with acute myeloid leukemia (Tsuchiya *et al.* 1980), are widely used as model systems for immunomodulation studies including drug and natural product testing (Schultze *et al.* 2017). At the same time, THP-1 is a cell line widely used in the investigations of acute myeloid leukemia (Lübbert *et al.* 1992).

Genetically encoded fluorescent protein sensors have provided major advances in cellular H_2O_2 detection (Bilan and Belousov 2018; Morgan *et al.* 2016). These probes contain a dithiol switch that changes the overall fluorescence of the probe depending on its oxidation status. High sensitivity and specificity for H_2O_2 have been achieved by coupling a redox-sensitive green fluorescent protein (GFP) mutant to a H_2O_2-sensitive thiol protein, such as oxyR (HyPer series) (Bilan and Belousov 2018), or to a peroxidase such as Orp1 or TSA2 (roGFP2-based probes) (Morgan *et al.* 2016). Among the several biosensors, HyPer7 is a pH-insensitive, genetically encoded H_2O_2 reporter, which consists of a cyclically permutated GFP with N- and C-terminal OxyR-RD domain derived from *Neisseria meningitidis* (Pak *et al.* 2020). Following oxidation by H_2O_2, HyPer7 forms an intramolecular disulfide bridge that alters the excitation spectra, and the maximum excitation of the HyPer7 chromophore shifts from 405 nm in the reduced state to 488 nm in the H_2O_2-oxidized state (Pak *et al.* 2020; Yang *et al.* 2023). Here, we constructed real-time, dynamic, and highly sensitive live-cell biosensors to monitor the cytosolic and mitochondrial H_2O_2 dynamics in a leukemia cell line THP-1, utilizing Hyper7 fused with subcellular localization guide peptides mitochondria localization sequence (MLS) and nuclear exclusion sequence (NES) to monitor cytosolic and mitochondrial H_2O_2 dynamics respectively in THP-1 cells, aiming to provide a powerful tool for detecting cytosolic and mitochondrial H_2O_2 in response to nanozymes.

MATERIALS AND METHODS

Cell culture

THP-1 cells were purchased from the Cell Resource Center of the Chinese Academy of Medical Sciences (Beijing, China) and cultured in modified RPMI medium (HyClone, Cytiva, Logan, Utah, USA) supplemented with 10% fetal bovine serum (FBS, Gibco, Thermo Fisher Scientific, Carlsbad, CA, USA), and 100 μg/mL penicillin-streptomycin (HyClone) in a humidified atmosphere of 5% CO_2 at 37°C. HEK 293T cells were cultured in DMEM (Gibco) supplemented with 10% FBS.

Construction of cell lines

HyPer7 was fused at the N–terminal of the protein with nuclear export sequence (NES, NSNELALKLAGLDINK) and mitochondrial localization sequence (MLS, MSVLTPLLLRGLTGSARRLPVPRAKIHSL) to express the sensor in the cytosol (CytoHyPer7), mitochondria (MitoHyPer7) of the cell, respectively. In brief, The THP-1 cells constructively expressed CytoHyPer7 and MitoHyPer7 were established by infecting with lentiviral carry the sequences. To obtain lentiviral, the sensor vectors (pLVX-NES-HyPer7, pLVX-MLS-HyPer7) together with three lentiviral packaging vectors (pLPI, pLPII, and pLPVSVG) were used to transfect HEK 293T cells at 50%–60% confluency by Lipofectamine 3000 (Invitrogen, USA) according to the manufacturer's instructions. The culture supernatant containing recombinant lentivirus was harvested after 72 h. Then THP-1 cells were seeded in six-well culture plates for lentiviral infection in the presence of 4 μg/mL of polybrene (Macgene, Beijing, China) followed by centrifugation at 1000*g* for 1 h at 37°C. Following the lentivirus infection, cells were cultured for 1 week in media containing 3 μg/mL puromycin. Afterward, the fluorescent cells were sorted by FACS Aria IIIu (BD Biosciences, Franklin Lakes, NJ, USA).

Nanozymes

Nanozymes used in this study included Prussian Blue Nanoparticles (PBNPs) and Fe_3O_4 nanoparticles, PtNPs, Au@Pt MnO_2, and MnBTC. PBNPs of 3.4 nm, referred to as ultrasmall Prussian Blue Nanoparticles (USPBNPs) were synthesized according to the procedure described previously (Qin *et al.* 2020). Briefly, to prepare PBNPs, 0.75 g of PVP and 0.0275 g of $K_3[Fe(CN)_6]$ were dissolved in 10 mL of ethanol solution. After stirring at room temperature for half an hour, the mixture was heated at 80°C for 20 h. The blue product was collected by centrifugation and washed several times with double-distilled water (ddH_2O). PBNPs, PEI- and Dex-modified Fe_3O_4 nanoparticles were purchased from Nanjing NanoEast Biotech Co. LTD. Transmission electron microscopy (TEM) and Dynamic Light Scatter (DLS) were utilized to characterize the shape, size, and Zeta potential of the nanoparticles, TEM images of Fe_3O_4 were provided by the supplier. PtNPs and Au@Pt were synthesized by the methods described previously (Wen *et al.* 2020). MnO_2 and MnBTC were kindly gifted by Prof. Lianbing Zhang (Chen *et al.* 2024).

Fluorescence microscope

Fluorescence microscopes were utilized to observe the intracellular location of HyPer7. For THP-1-Mito-HyPer-7, the cells were stained with 200 nmol/L MitoTracker® Red CMXRos (#M7512, Invivogen) for 20 min according to the instructions before fixing. Both cells were then fixed with 1 mL of 100% pre-cooled methanol for 10 min and washed with PBS. The cells were then resuspended with 1 mL of PBS, and 200 μL of the cell suspension was subjected to cytospin. The cells were mounted with a mounting medium containing DAPI (#ZLI-9556, Zhongshan Golden Bridge) and covered with a coverslip for observation. The slides were observed and photographed using a confocal microscope (Leica TCS SP8 STED, Leica) under the conditions of *Ex*/*Em* = 350/450 nm (For DAPI), 488/525 nm (For HyPer7), and 577/602 nm (For MitoTracker® Red).

Flow cytometry

To detect the responsiveness of the biosensors to exogenous H_2O_2, THP-1-CytoHyPer7 cells and THP-1-MitoHyPer7 cells with a density of 4×10^5 cell/mL were treated with H_2O_2 (10011218, Sinopharm Chemical Reagent Co., Ltd.) at concentrations ranging from 1 μmol/L to 400 μmol/L for 2 min. The fluorescence in the cells was detected by flow cytometry (CytoFLEX, Beckman Coulter) using 405 and 488 nm as excitation lights and collecting the emission light through 525/50 nm and 530/30 nm bandpass filters, respectively. Imaging flow cytometry (ImageStream^X Mark Ⅱ, Merk) was also used to photograph the emission fluorescence at 525 nm upon 488 nm excitation after being incubated with 100 μmol/L H_2O_2.

To monitor the dynamics of cytosolic and mitochondrial H_2O_2 induced by chemotherapeutics reagents and nanozymes, THP-1-CytoHyPer7 cells and THP-1-MitoHyPer7 cells with a density of 4×10^5 cell/mL were incubated with different concentrations of

chemotherapeutics reagents and nanozymes. After co-incubation for 6, 24, and 48 h, the cells were collected by centrifugation, washed once with PBS, and detected by flow cytometry. The experimental data were analyzed using FlowJo (V10).

Statistics

All data were expressed as the mean ± standard deviation (SD) for at least triplicate experiments. Statistical analysis was performed in Graphpad Prism 8.3.0. To compare the means of three or more groups defined by one factor, One-way ANOVA was employed and followed by Dunnett post-hoc test to compare the means of a prespecified pair of columns. $P < 0.05$ is considered statistically significant.

RESULTS AND DISCUSSION

Cytosolic and mitochondrial localization of Hyper7 probe in THP-1 cells

Hyper7 has been widely employed as H_2O_2 biosensors in model organisms including yeasts (de Cubas *et al.* 2021; Kritsiligkou *et al.* 2021, 2023), *Arabidopsis thaliana* (Dopp *et al.* 2023), *Mus musculus* (Kano *et al.* 2024; Li *et al.* 2022), Zebrafish *Danio rerio* (Sergeeva *et al.* 2025), as well as cell lines in culture including human umbilical vein endothelial cells (HUVEC) (Jacobs *et al.* 2022; Waldeck-Weiermair *et al.* 2022), mouse hepatocytes (AML12 cells) (Shashkovskaya *et al.* 2023), hippocampal neurons (Kotova *et al.* 2023), human iPCs derived spheroids (Usatova *et al.* 2024). In this study, we applied Hyper7 to monitor the dynamics of cytosolic and mitochondrial H_2O_2 in THP-1 cells. The cells expressing Cyto-Hyper7 (upper column in Fig. 1) exclusively exhibited a uniform cytosolic distribution of fluorescent protein sensor signals (green in Fig. 1) compared to the DAPI-stained nucleus (blue in Fig. 1). Mito-Hyper7 (down column in Fig. 1) was intended to target the mitochondria and colocalize with Mito-Tracker Red (red in Fig. 1), and the PCC between the Mito-HyPer7 probe and MitoTracker signal was recorded as 0.90, indicating a collocation. These images clearly confirmed the correct distribution of Cyto-HyPer7 and Mito-HyPer7 in the cytosol and mitochondria, and the successful construction of the biosensors.

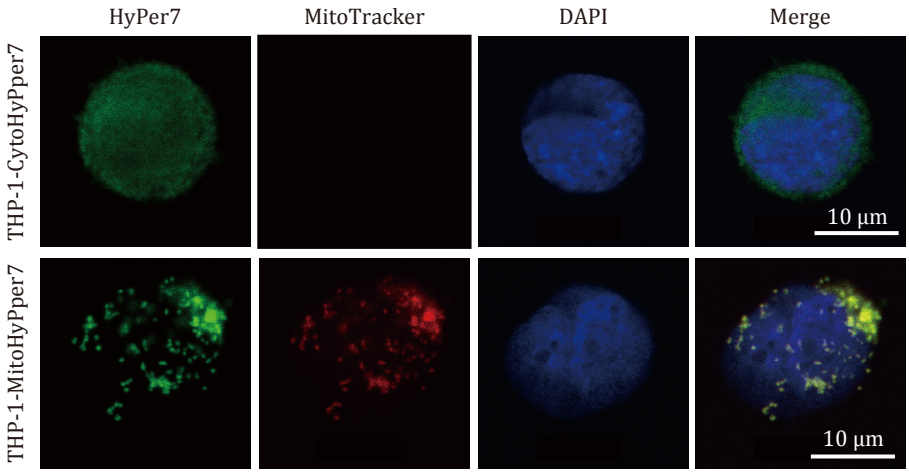

Fig. 1 Targeting expression of HyPer7 probe in cytosol and mitochondria. Scale bar = 10 μm

Responsiveness of the biosensors to exogenously added hydrogen peroxide

H_2O_2 can diffuse from extracellular space into cytosol and further into mitochondria (Pak *et al.* 2020). To verify whether the biosensors can respond to the perturbation of H_2O_2, we added exogenously H_2O_2 to the culture medium, and results showed that externally added H_2O_2 caused a detectable oxidation of both probes. Upon oxidation, the excitation spectra of HyPer7 changed with a decrease at 405 nm and an increase of the 488 nm peak, while the emission spectra are similar in both states, peaking at 525 nm (Fig. 2A). Therefore, we detected fluorescence upon the

excitation with lasers of 405 nm (referred to as F405) and 488nm (referred to as F488). It was shown that the fluorescence upon 405 nm excitation was reduced while that upon 488 nm was increased when the cells were incubated with exogenous H_2O_2 (Figs. 2B and 2C). Images acquired from the imaging flow cytometry (Figs. 2D and 2E) supported the results of flow cytometry, showing that the fluorescence of the cells exposed to 100 μmol/L H_2O_2 was brighter than that of the control cells.

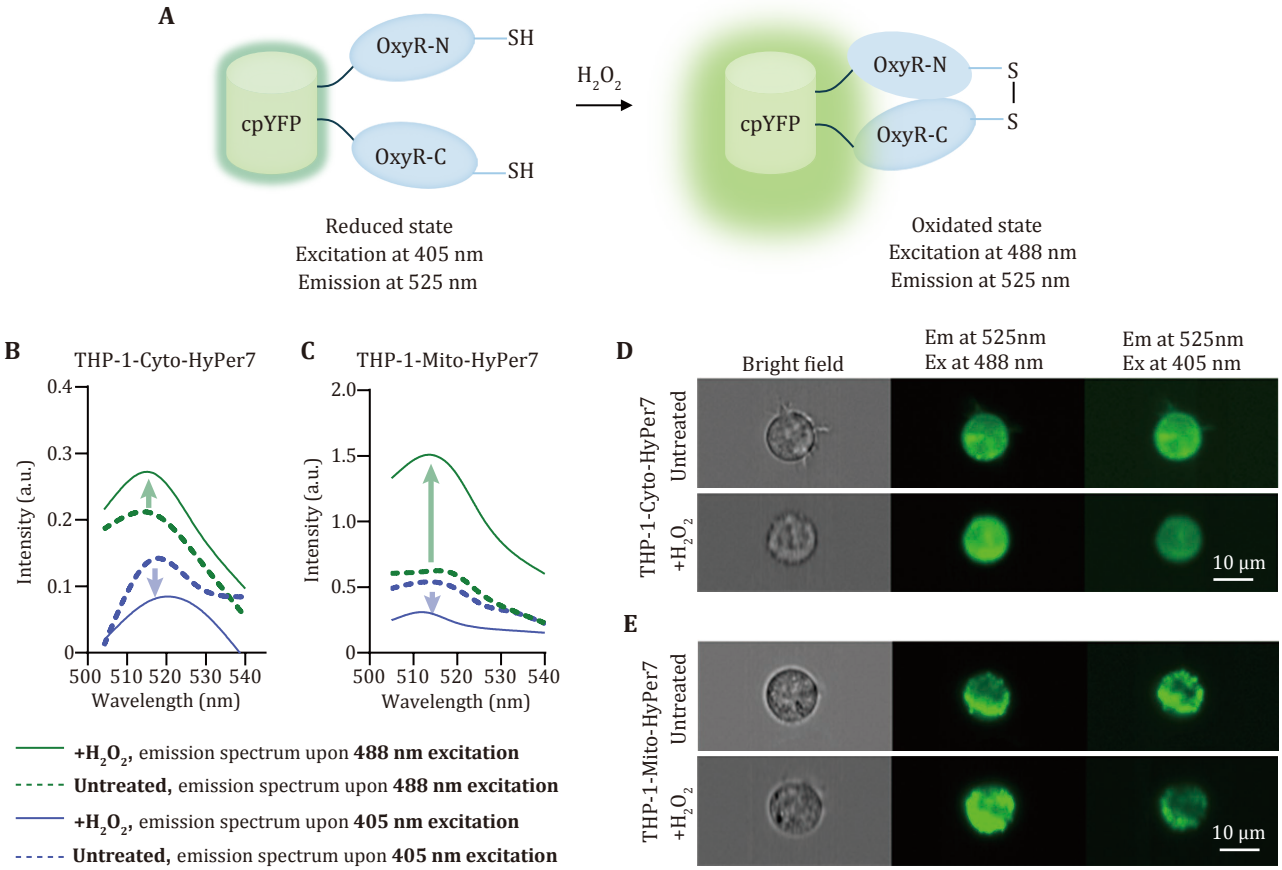

Fig. 2 Fluorescence shift of the biosensors in response to exogenously adding H_2O_2. **A** Illustration of the mechanism of Hyper7 probe in response to H_2O_2. **B**,**C** Emission spectrum of THP-1-CytoHyPper7 cells (**B**) and THP-1-MitoHyPper7 cells (**C**) upon 405 nm (purple lines) and 488 nm (green lines) excitation, the dotted line indicated untreated group, while the solid line indicated cells co-incubation with H_2O_2. **D**,**E** Fluorescence at 525 nm upon 488 nm excitation and 405 nm excitation in THP-1-CytoHyper7 cells (**D**) and THP-1-MitoHyper7 cells (**E**), captured by imaging flow cytometry, scale bar =10 μm

Having confirmed that HyPer7 is expressed and responsive, we performed a titration experiment to determine the minimal amount of exogenous H_2O_2 that is required to elicit a detectable probe response and the maximal detectable H_2O_2 concentration. We used flow cytometry to evaluate the variation in fluorescence intensity after co-incubation with H_2O_2. For THP-1-CytoHyPer7, the minimal detectable amount of exogenous H_2O_2 was 10 μmol/L, and F488 increased along with the climb of the H_2O_2 concentration when the concentration of exogenous H_2O_2 ranged from 10 to 40 μmol/L, and when the exogenous H_2O_2 concentration exceeds 40 μmol/L, the fluorescence intensity reached a plateau without further enhancement (Fig. 3A). For THP-1-MitoHyPer7, the minimal detectable amount of exogenous H_2O_2 was 10 μmol/L, and the detectable range was 10 to 100 μmol/L (Fig. 3B). To make it simpler, we used the normalized fluorescence ratio of F488 to F405 (F488/F405) to characterize the relative H_2O_2 compared to the untreated cells (Figs. 3C and 3D), the maximal F488/F405 of THP-1-CytoHyPer7 and THP-1-MitoHyPer7 reached 6.83 and 9.49, respectively.

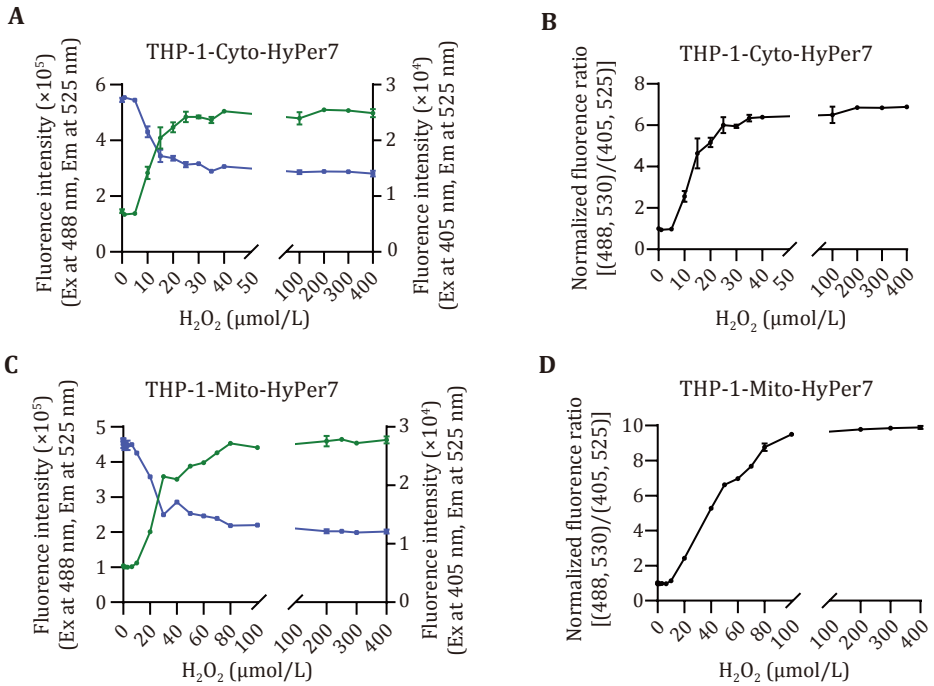

Fig. 3 Dosage effects of the biosensors in response to exogenously adding H_2O_2. **A**, **B** Fluorescence intensity of THP-1-CytoHyPper7 cells (**A**) and THP-1-MitoHyPper7 cells (**B**) after being treated with H_2O_2 of gradient concentration upon 405 nm (purple) excitation and 488 nm (green). **C**,**D** Normalized fluorescence Ratio of THP-1-CytoHyPper7 cells (**C**) and THP-1-MitoHyPper7 cells (**D**) after being treated with H_2O_2 of gradient concentration

Monitor H_2O_2 level in response to chemotherapeutic agents

Most chemotherapeutic agents were reported to induce intracellular ROS accumulation through several mechanisms. Herein, we employed Daunorubicin (DNR) to monitor the dynamics of cytosolic and mitochondrial H_2O_2. It is well known that DNR plays its cytotoxicity by increasing intracellular ROS (Burt *et al.* 2019), however, the subcellular compartment of ROS generation was unclear. Our results from the CCK8 assay indicated the IC_{50} at 24 h was 161.4 nmol/L (Fig. 4A). By using the biosensors established in this study, we found out that in the dose range of 20 nmol/L to 200 nmol/L, the cytosolic and mitochondrial H_2O_2 remained unchanged after treated for 6 h and 24 h (Figs. 4B and 4C). Only a slight increase of F488/F405 was observed in the cytosolic H_2O_2 after treated for 48 h while a dramatic increase of 1.55 folds was observed in the mitochondrial H_2O_2 (Fig. 4D). It should be noted that in the 6-h experiment, dosages were increased up to 1.5 mmol/L. Results showed that the high doses of DNR increased cytosolic and mitochondrial H_2O_2 at the same time, and 1.5 mmol/L of DNR resulted in 1.33 folds and 1.21 folds of cytosolic and mitochondrial H_2O_2 compared with the untreated cells, respectively. These results indicated the long-term effects on H_2O_2 occurred primarily in mitochondria while the short-term and high-dose effects occurred in both mitochondria and cytosol. Moreover, the increase of cytosolic H_2O_2 induced by DNR could be partly reversed by N-acetylcysteine (NAC), indicating that the sensor cells were capable of sensing and detecting the attenuation of H_2O_2 induced by antioxidant (Fig. 4E).

Since ROS has been identified as one of the common mediators for chemo-resistance in leukemia (Trombetti *et al.* 2021), the constructed biosensors offer a powerful platform to monitor the dynamic of cytosolic and mitochondrial H_2O_2 in resistant or sensitive cells and to continuously monitor the adjustment of H_2O_2, which will be helpful to reveal the mechanism of chemotherapy resistance in leukemia.

Monitor H_2O_2 level in response to nanozymes

Next, we applied the biosensors to monitor H_2O_2 dynamics after co-incubation with several nanozymes that have multi-enzyme properties to affect intracellular H_2O_2 concentrations. Fe_3O_4 nanoparticle was the first nanozyme reported with POD-like activity (Gao *et al.* 2007), and further investigations revealed its POD-like activity under the acidic environment (pH = 4.8) and

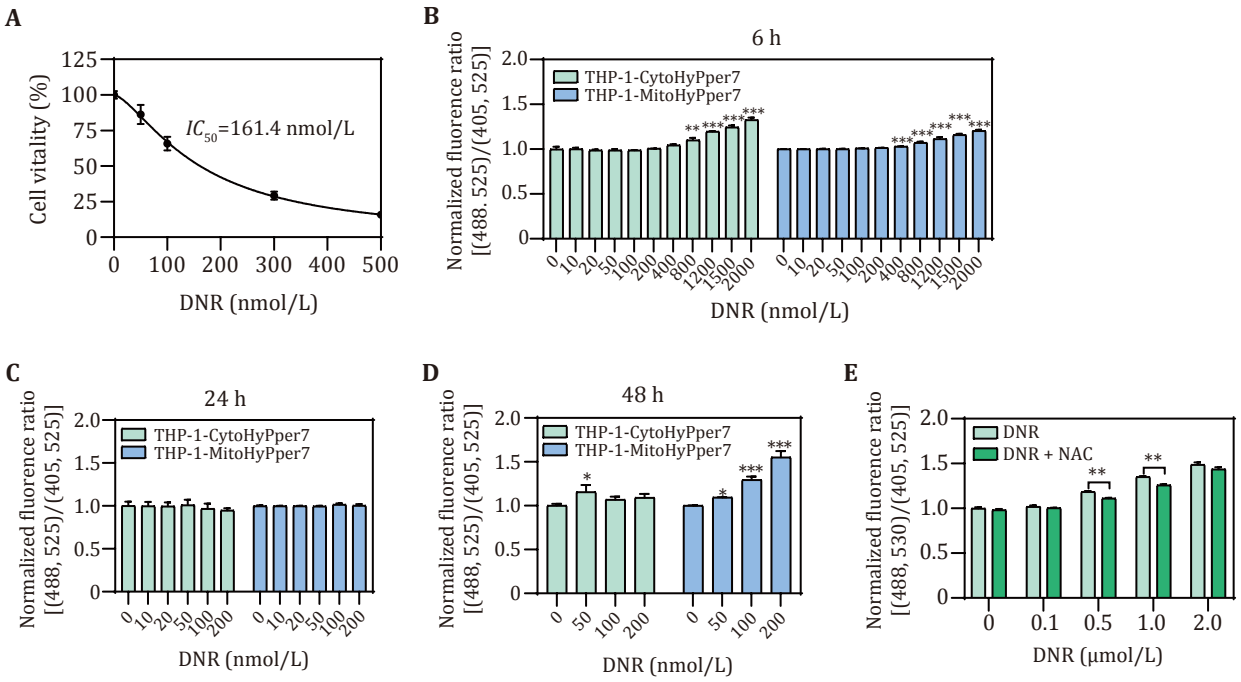

Fig. 4 Detection of cytosolic and mitochondrial H_2O_2 perturbation after incubation with DNR. **A** Cell viability of THP-1 cells after incubation with DNR for 24 h. **B** Normalized fluorescence ratio of THP-1-CytoHyPper7 cells (green) and THP-1-MitoHyPper7 cells (blue) after being treated with DNR for 6 h. **C** Normalized fluorescence ratio of THP-1-CytoHyPper7 cells after being treated with DNR in the presence or absence of NAC for 6 h. **D**,**E** Normalized fluorescence ratio of THP-1-CytoHyPper7 cells (green) and THP-1-MitoHyPper7 cells (blue) after being treated with DNR for 24 h (**D**), and 48 h (**E**)

CAT-like activity in neutral conditions (pH = 7.4) (Chen *et al.* 2012). Herein, by using the biosensors, we detected the dynamics of cytosolic and mitochondrial H_2O_2 after incubation with Fe_3O_4 nanoparticles coated with PEI (referred to as PEI-Fe_3O_4) and Dextran (referred to as Dex-Fe_3O_4). The diameters of both Fe_3O_4 nanoparticles were less than 20 nm under TEM (Figs. 5A and 5B). Their hydrodynamic diameters were 46.57 ± 1.31 nm and 27.95 ± 1.29 nm determined by DLS. Dex-Fe_3O_4 was negatively charged with zeta potentials of −20.29 ± 5.00 mV, while PEI-Fe_3O_4 was positively charged with zeta potentials of 13.18 ± 3.39 mV. After co-incubation with Dex-Fe_3O_4 for 6 h, cytosolic and mitochondrial H_2O_2 were scavenged at the same time and decreased further after 24 h (Figs. 5C–5E). PEI-Fe_3O_4 acted differently from Dex-Fe_3O_4. The variation in mitochondrial H_2O_2 was less than 1% after incubation with PEI-Fe_3O_4 for 6 h, which can be considered unchanged (Fig. 5F). At the same time, the variation of cytosolic H_2O_2 was uncommon, that was, it decreased by 5% upon being treated with 10 mg/L PEI-Fe_3O_4, while as the concentration climbed to 20 mg/L and 40 mg/L, H_2O_2 gradually rose and became comparable to the control group in the 40 mg/L PEI-Fe_3O_4 group (Fig. 5F). After co-incubation for 24 h, the cytosolic H_2O_2 was diminished compared to the untreated cells (Fig. 5G). As the incubation time was extended to 48 h, the concentration of mitochondrial H_2O_2 decreased too (Fig. 5H). Therefore, it is plausible to consider that the overall H_2O_2 was attributed to both the nanozyme's properties and the surface modification of the nanoparticles.

Surface modification-dependent effects (Fig. 5) highlight the need for quick screening for the intracellular effects of nanozymes, especially those that could modulate ROS. The biosensors provide a standardized system to guide surface engineering to minimize unintended ROS modulation.

PBNPs were reported for their ability of scavenging ROS both in tubes as well as in cells (Zhang *et al.* 2016). In this study, we detect the intracellular effects of two PBNPs with different diameters by using the established biosensors. The Prussian Blue nanoparticles exhibit a sub-spherical shape under TEM with a diameter of about 60 nm, and the hydrodynamic diameter was determined to be 92.23 ± 4.33 nm (Fig. 6A). Ultrasmall Prussian Blue nanoparticles exhibit a cluster-like shape under TEM with a diameter of about 5 nm, and the hydrodynamic diameter was determined to be 34.73 ± 7.96 nm (Fig. 6B). PBNPs and

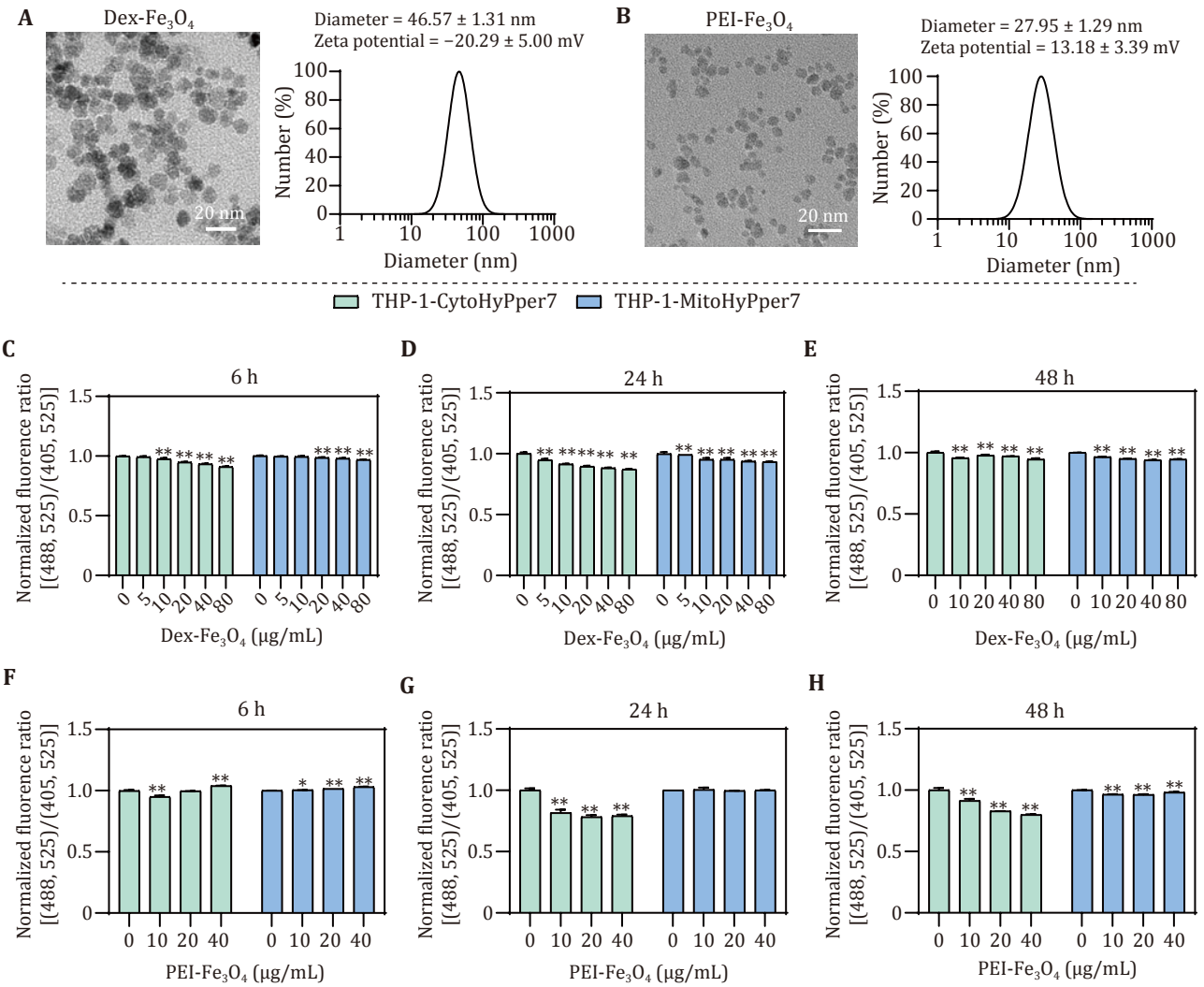

Fig. 5 Detection of cytosolic and mitochondrial H_2O_2 perturbation after incubation with Dex-Fe_3O_4 and PEI-Fe_3O_4. **A**,**B** Size of Dex-Fe_3O_4 (**A**) and PEI-Fe_3O_4 (**B**) under TEM and the hydrodynamic diameter distributions in ddH_2O measured by DLS. **C**–**E** Normalized fluorescence ratio of THP-1-CytoHyPper7 cells (green) and THP-1-MitoHyPper7 cells (blue) after being treated with Dex-Fe_3O_4 for 6 h (**C**), 24 h (**D**), and 48 h (**E**). **F**–**H** Normalized fluorescence ratio of THP-1-CytoHyPper7 cells (green) and THP-1-MitoHyPper7 cells (blue) after being treated with PEI-Fe_3O_4 for 6 h (**F**), 24 h (**G**), and 48 h (**H**)

USPBNPs were both negatively charged with zeta potentials of −12.08 ± 0.97 mV and −40.71 ± 1.43 mV, respectively. We found out that the PBNPs didn't change cytosolic or mitochondrial H_2O_2 after 6 h incubation and eventually scavenged H_2O_2 by 13% after being treated for 48 h (Figs. 6C–6E). However, it is interesting to see that USPBNPs exhibited different overall effects on the intracellular H_2O_2. The cytosolic and mitochondrial H_2O_2 was elevated upon co-incubation with USPBNPs (Figs. 6F–6H), which suggested that the particle size of nanozyme also played a role in regulating intracellular H_2O_2, though the high POD-like and CAT-like activities were demonstrated in USPBNPs over PBNPs.

Mn-based and Pt-based nanozymes were also detected with the biosensors. After co-incubation for 24 h, the PtNPs caused an increase in both cytosolic and mitochondrial H_2O_2. MnO_2 and Au@Pt decreased cytosolic H_2O_2 without changing mitochondrial H_2O_2, while MnBTC increased mitochondrial H_2O_2 without changing cytosolic H_2O_2 (Fig. 7).

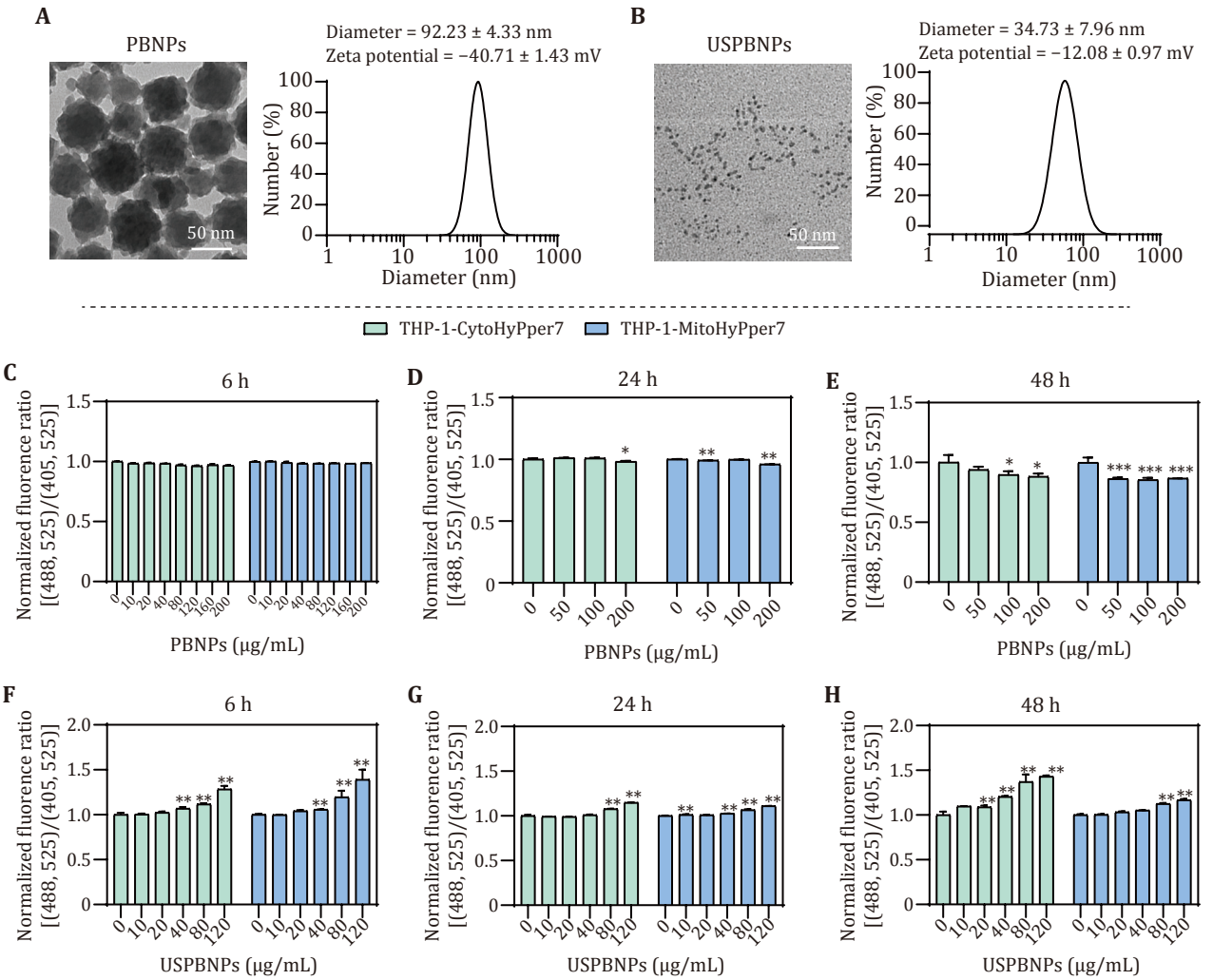

Fig. 6 Detection of cytosolic and mitochondrial H_2O_2 perturbation after incubation with PBNPs and USPBNPs. **A**,**B** Size of PBNPs (**A**) and USPBNPs (**B**) under TEM and their hydrodynamic diameter distribution in ddH_2O determined by DLS. **C**–**E** Normalized fluorescence ratio of THP-1-CytoHyPer7 cells (green) and THP-1-MitoHyPer7 cells (blue) after being treated with PBNPs for 6 h (**C**), 24 h (**D**), and 48 h (**E**). **F**–**H** Normalized fluorescence ratio of THP-1-CytoHyPer7 cells (green) and THP-1-MitoHyPer7 cells (blue) after being treated with USPBNPs for 6 h (**F**), 24 h (**G**), and 48 h (**H**)

CONCLUSION

In summary, this work constructed the genetically encoded fluorescent sensors CytoHyper7 and MitoHyper7 to detect cytosolic and mitochondrial H_2O_2 levels. The performance of the sensors was characterized by fluorescent spectroscopy, and the responses to chemotherapeutics DNR and nanozymes of PBNPs with different diameters and iron oxide nanoparticles with different surface modifications were revealed. Results obtained by using the biosensors indicated that the particle size of PBNPs and surface modification of Fe_3O_4 play critical roles in their intracellular effects on the aspect of H_2O_2 modulation.

Acknowledgements This work was supported by the National Key R&D Program of China (2022YFA1205800, 2022YFC2303501), and the National Natural Science Foundation of China (32471461, 82402471).

Compliance with Ethical Standards

Conflict of interest Haiyan Xu, Dianbing Wang, Tao Wang, Mengfan Yu, Chenshuo Ren, Fan Yang, Tao Wen, Xian-En Zhang, Haoan Wu and Yu Zhang declare that they have no conflict of interest.

Human and animal rights and informed consent This article does not contain any studies on human or animal subjects.

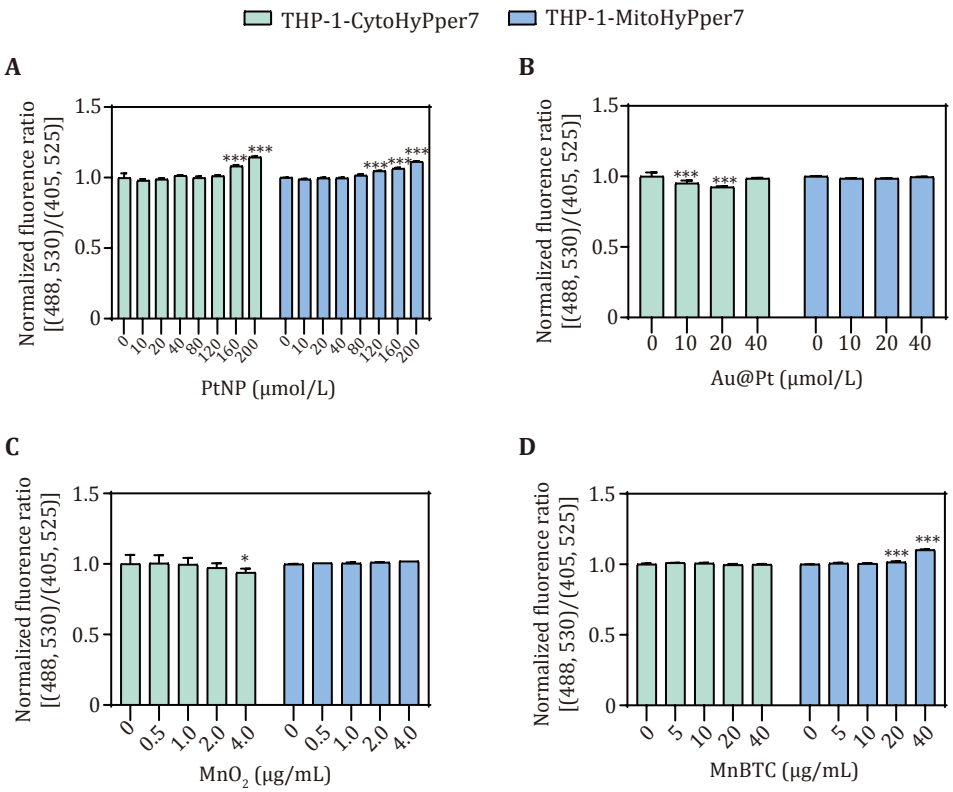

Fig. 7 Normalized fluorescence ratio of THP-1-CytoHyPper7 cells and THP-1-MitoHyPper7 cells after incubation with PtNPs (**A**), Au@Pt (**B**), MnO_2 (**C**), MnBTC (**D**) nanozymes for 24 h

References

Bedard K, Krause KH (2007) The NOX family of ROS-generating NADPH oxidases: physiology and pathophysiology. Physiol Rev 87(1): 245–313

Bilan DS, Belousov VV (2018) *In vivo* imaging of hydrogen peroxide with HyPer probes. Antioxid Redox Signal 29(6): 569–584

Burt R, Dey A, Aref S, Aguiar M, Akarca A, Bailey K, Day W, Hooper S, Kirkwood A, Kirschner K, Lee SW, Lo Celso C, Manji J, Mansour MR, Marafioti T, Mitchell RJ, Muirhead RC, Cheuk Yan Ng K, Pospori C, Puccio I, Zuborne-Alapi K, Sahai E, Fielding AK (2019) Activated stromal cells transfer mitochondria to rescue acute lymphoblastic leukemia cells from oxidative stress. Blood 134(17): 1415–1429

Chen Y, Tian Q, Wang HY, Ma RN, Han RT, Wang Y, Ge HB, Ren YJ, Yang R, Yang HM, Chen YJ, Duan XZ, Zhang LB, Gao J, Gao LZ, Yan XY, Qin Y (2024) A manganese-based metal-organic framework as a cold-adapted nanozyme. Adv Mater 36(10): 2206421. https://doi.org/10.1002/adma.202206421

Chen ZW, Yin J-J, Zhou Y-T, Zhang Y, Song LN, Song MJ, Hu SL, Gu N (2012) Dual enzyme-like activities of iron oxide nanoparticles and their implication for diminishing cytotoxicity. ACS Nano 6(5): 4001–4012

D'Autréaux B, Toledano MB (2007) ROS as signalling molecules: mechanisms that generate specificity in ROS homeostasis. Nat Rev Mol Cell Biol 8(10): 813–824

de Cubas L, Pak VV, Belousov VV, Ayté J, Hidalgo E (2021) The mitochondria-to-cytosol H_2O_2 gradient is caused by peroxiredoxin-dependent cytosolic scavenging. Antioxidants 10(5): 731. https://doi.org/10.3390/antiox10050731

Dopp IJ, Kalac K, Mackenzie SA (2023) Hydrogen peroxide sensor HyPer7 illuminates tissue-specific plastid redox dynamics. Plant Physiol 193(1): 217–228

Gao LZ, Zhuang J, Nie L, Zhang JB, Zhang Y, Gu N, Wang TH, Feng J, Yang DL, Perrett S, Yan XY (2007) Intrinsic peroxidase-like activity of ferromagnetic nanoparticles. Nat Nanotechnol 2(9): 577–583

Guan JY, Dong D, Khan NA, Zheng Y (2024) Emerging Pt-based intermetallic nanoparticles for the oxygen reduction reaction. Chem Commun 60(14): 1811–1825

Jacobs LJHC, Hoehne MN, Riemer J (2022) Measuring intracellular H_2O_2 in intact human cells using the genetically encoded fluorescent sensor HyPer7. Bio Protoc 12(20): e4538. https://doi.org/10.21769/BioProtoc.4538

Jiang DW, Ni DL, Rosenkrans ZT, Huang P, Yan XY, Cai WB (2019) Nanozyme: new horizons for responsive biomedical applications. Chem Soc Rev 48(14): 3683–3704

Kano R, Kusano T, Takeda R, Shirakawa H, Poole DC, Kano Y, Hoshino D (2024) Eccentric contraction increases hydrogen peroxide levels and alters gene expression through Nox2 in skeletal muscle of male mice. J Appl Physiol 137(3): 778–788

Kotova DA, Ivanova AD, Pochechuev MS, Kelmanson IV, Khramova YV, Tiaglik A, Sudoplatov MA, Trifonova AP, Fedotova A, Morozova K, Katrukha VA, Sergeeva AD, Raevskii RI, Pestriakova MP, Solotenkov MA, Stepanov EA, Tsopina AS, Moshchenko AA, Shestopalova M, Zalygin A, Fedotov IV, Fedotov AB, Oleinikov V, Belousov VV, Semyanov A, Brazhe N, Zheltikov AM, Bilan DS (2023) Hyperglycemia exacerbates ischemic stroke not through increased generation of hydrogen peroxide. Free Radic Biol Med 208: 153–164

Kritsiligkou P, Shen TK, Dick TP (2021) A comparison of Prx- and OxyR-based H_2O_2 probes expressed in *S. cerevisiae*. J Biol Chem 297(1): 100866. https://doi.org/10.1016/j.jbc.2021.100866

Kritsiligkou P, Bosch K, Shen TK, Meurer M, Knop M, Dick TP (2023) Proteome-wide tagging with an H_2O_2 biosensor reveals highly localized and dynamic redox microenvironments. Proc Natl Acad Sci USA 120(48): e2314043120. https://doi.org/10.1073/pnas.2314043120

Li XY, Zhang YY, Ai HW (2022) Ratiometric imaging of mitochondrial hydrogen peroxide in $A\beta_{42}$-mediated neurotoxicity. ACS Sens 7(3): 722–729

Lübbert M, Mertelsmann R, Herrmann F (1992) Detection of allele-specific expression of N-RAS oncogenes in human leukaemia cells. Br J Haematol 81(3): 370–373

Morgan B, Van Laer K, Owusu TNE, Ezeriņa D, Pastor-Flores D, Amponsah PS, Tursch A, Dick TP (2016) Real-time monitoring of basal H_2O_2 levels with peroxiredoxin-based probes. Nat Chem Biol 12(6): 437–443

Murphy MP (2009) How mitochondria produce reactive oxygen species. Biochem J 417(1): 1–13

Murphy MP, Bayir H, Belousov V, Chang CJ, Davies KJA, Davies MJ, Dick TP, Finkel T, Forman HJ, Janssen-Heininger Y, Gems D, Kagan VE, Kalyanaraman B, Larsson NG, Milne GL, Nyström T, Poulsen HE, Radi R, Van Remmen H, Schumacker PT, Thornalley PJ, Toyokuni S, Winterbourn CC, Yin HY, Halliwell B (2022) Guidelines for measuring reactive oxygen species and oxidative damage in cells and *in vivo*. Nat Metab 4(6): 651–662

Pak VV, Ezeriņa D, Lyublinskaya OG, Pedre B, Tyurin-Kuzmin PA, Mishina NM, Thauvin M, Young D, Wahni K, Martínez Gache SA, Demidovich AD, Ermakova YG, Maslova YD, Shokhina AG, Eroglu E, Bilan DS, Bogeski I, Michel T, Vriz S, Messens J, Belousov VV (2020) Ultrasensitive genetically encoded indicator for hydrogen peroxide identifies roles for the oxidant in cell migration and mitochondrial function. Cell Metab 31(3): 642–653. e6

Parvez S, Long MJC, Poganik JR, Aye Y (2018) Redox signaling by reactive electrophiles and oxidants. Chem Rev 118(18): 8798–8888

Qin ZG, Chen B, Mao Y, Shi C, Li Y, Huang X, Yang F, Gu N (2020) Achieving ultrasmall prussian blue nanoparticles as high-performance biomedical agents with multifunctions. ACS Appl Mater Interfaces 12(51): 57382–57390

Ren XY, Chen DX, Wang Y, Li HF, Zhang YB, Chen HY, Li X, Huo MF (2022) Nanozymes-recent development and biomedical applications. J Nanobiotechnol 20(1): 92. https://doi.org/10.1186/s12951-022-01295-y

Schultze N, Wanka H, Zwicker P, Lindequist U, Haertel B (2017) Mitochondrial functions of THP-1 monocytes following the exposure to selected natural compounds. Toxicology 377: 57–63

Sergeeva AD, Panova AS, Ivanova AD, Khramova YV, Morozova KI, Kotova DA, Guryleva AV, Khokhlov DD, Kelmanson IV, Vasilev AV, Kostyuk AI, Semyanov AV, Oleinikov VA, Belousov VV, Machikhin AS, Brazhe NA, Bilan DS (2025) Where in the tissues of *Danio rerio* is more H_2O_2 produced during acute hypoxia? Antioxid Redox Signal 42(4–6): 292–300

Shashkovskaya VS, Vetosheva PI, Shokhina AG, Aparin IO, Prikazchikova TA, Mikaelyan AS, Kotelevtsev YV, Belousov VV, Zatsepin TS, Abakumova TO (2023) Delivery of lipid nanoparticles with ROS probes for improved visualization of hepatocellular carcinoma. Biomedicines 11(7): 1783. https://doi.org/10.3390/biomedicines11071783

Sies H, Jones DP (2020) Reactive oxygen species (ROS) as pleiotropic physiological signalling agents. Nat Rev Mol Cell Biol 21(7): 363–383

Sies H, Belousov VV, Chandel NS, Davies MJ, Jones DP, Mann GE, Murphy MP, Yamamoto M, Winterbourn C (2022) Defining roles of specific reactive oxygen species (ROS) in cell biology and physiology. Nat Rev Mol Cell Biol 23(7): 499–515

Sies H, Mailloux RJ, Jakob U (2024) Fundamentals of redox regulation in biology. Nat Rev Mol Cell Biol 25(9): 701–719

Trombetti S, Cesaro E, Catapano R, Sessa R, Lo Bianco A, Izzo P, Grosso M (2021) Oxidative stress and ROS-mediated signaling in leukemia: novel promising perspectives to eradicate chemoresistant cells in myeloid leukemia. Int J Mol Sci 22(5): 2470. https://doi.org/10.3390/ijms22052470

Tsuchiya S, Yamabe M, Yamaguchi Y, Kobayashi Y, Konno T, Tada K (1980) Establishment and characterization of a human acute monocytic leukemia cell line (THP-1). Int J Cancer 26(2): 171–176

Usatova VS, Mishina NM, Berestovoy MA, Ivanenko AV, Jappy D, Krut' VG, Sokolov RA, Moshchenko AA, Rozov A, Shevchenko EK, Belousov VV (2024) Hydrogen peroxide is not generated intracellularly in human neural spheroids during ischemia-reperfusion. Free Radic Biol Med 212: 234–240

Waldeck-Weiermair M, Yadav S, Kaynert J, Thulabandu VR, Pandey AK, Spyropoulos F, Covington T, Das AA, Krüger C, Michel T (2022) Differential endothelial hydrogen peroxide signaling via Nox isoforms: critical roles for Rac1 and modulation by statins. Redox Biol 58: 102539 https://doi.org/10.1016/j.redox.2022.102539

Wen T, Yang AY, Wang T, Jia MF, Lai XN, Meng J, Liu J, Han B, Xu HY (2020) Ultra-small platinum nanoparticles on gold nanorods induced intracellular ROS fluctuation to drive megakaryocytic differentiation of leukemia cells. Biomater Sci 8(22): 6204–6211

Yang EJN, Boldogh IR, Ji HJ, Pon L, Swayne TC (2023) Imaging of mtHyPer7, a ratiometric biosensor for mitochondrial peroxide, in living yeast cells. J Vis Exp 196: e65428. https://doi.org/10.3791/65428

Zhang W, Hu SL, Yin J-J, He WW, Lu W, Ma M, Gu N, Zhang Y (2016) Prussian blue nanoparticles as multienzyme mimetics and reactive oxygen species scavengers. J Am Chem Soc 138(18): 5860–5865